# Validation of 2-$^{18}$F-Fluorodeoxysorbitol as a Potential Radiopharmaceutical for Imaging Bacterial Infection in the Lung

Junling Li, Huaiyu Zheng, Ramy Fodah, Jonathan M. Warawa, and Chin K. Ng

*University of Louisville School of Medicine, Louisville, Kentucky*

2-$^{18}$F-fluorodeoxysorbitol ($^{18}$F-FDS) has been shown to be a promising agent with high selectivity and sensitivity in imaging bacterial infection. The objective of our study was to validate $^{18}$F-FDS as a potential radiopharmaceutical for imaging bacterial infection longitudinally in the lung. **Methods:** Albino C57 female mice were intratracheally inoculated with either live or dead *Klebsiella pneumoniae* to induce either lung infection or lung inflammation. One group of mice was imaged to monitor disease progression. PET/CT was performed on days 0, 1, 2, and 3 after inoculation using either $^{18}$F-FDS or $^{18}$F-FDG ($n = 12$ for each tracer). The other group was first screened by bioluminescent imaging (BLI) to select only mice with visible infection (region of interest $> 10^8$ ph/s) for PET/CT imaging with $^{18}$F-FDS ($n = 12$). For the inflammation group, 5 mice each were imaged with PET/CT using either $^{18}$F-FDS or $^{18}$F-FDG from days 1 to 4 after inoculation. **Results:** For studies of disease progression, BLI showed noticeable lung infection on day 2 after inoculation and significantly greater infection on day 3. Baseline imaging before inoculation showed no focal areas of lung consolidation on CT and low uptake in the lung for both PET radiotracers. On day 2, an area of lung consolidation was identified on CT, with a corresponding 2.5-fold increase over baseline for both PET radiotracers. On day 3, widespread areas of patchy lung consolidation were found on CT, with a drastic increase in uptake for both $^{18}$F-FDS and $^{18}$F-FDG (9.2 and 3.9). PET and BLI studies showed a marginal correlation between $^{18}$F-FDG uptake and colony-forming units ($r = 0.63$) but a much better correlation for $^{18}$F-FDS ($r = 0.85$). The uptake ratio of infected lung over inflamed lung was 8.5 and 1.7 for $^{18}$F-FDS and $^{18}$F-FDG on day 3. **Conclusion:** Uptake of both $^{18}$F-FDS and $^{18}$F-FDG in infected lung could be used to track the degree of bacterial infection measured by BLI, with a minimum detection limit of $10^7$ bacteria. $^{18}$F-FDS, however, is more specific than $^{18}$F-FDG in differentiating *K. pneumoniae* lung infection from lung inflammation.

**Key Words:** $^{18}$F-PET/CT; bacterial infection; sterile inflammation; disease progression

Bacterial infections cause significant mortality and morbidity worldwide despite the availability of antibiotics. In the United States alone, approximately 2 million patients develop a hospital-acquired infection each year. *Klebsiella pneumoniae* is a gram-negative, rod-shaped organism that is the fifth most prevalent nosocomial bacterial pathogen in the United States for infections associated with the urinary tract, ventilator associated pneumonia, and central line–associated bacteremia and accounts for 6% of all nosocomial bacterial disease (*1,2*). The conventional diagnosis of *K. pneumoniae* infection is derived from cultures of samples obtained from the site of suspected infection, which can take several days and may not provide reliable information since blood cultures can have high contamination rates. There are other clinical methods to identify infection, such as monitoring of body temperature, white blood cell count, erythrocyte sedimentation rate, and cytokine reactions, but none of these is a specific response to infection or able to differentiate bacterial infection from inflammation (*3*). In addition, the emergence of *K. pneumoniae* resistance to antimicrobial drug is well documented (*4*).

Noninvasive imaging can provide real-time in vivo monitoring of the progression of infection. Plain film (x-ray) radiography and CT have been useful for clinical assessments of *K. pneumoniae* infection severity but are limited by characterizing only anatomic changes in the lung parenchyma, such as ground-glass opacity and consolidations (*5*). In contrast, PET imaging with $^{18}$F-FDG has proven useful for imaging inflammation and infection, but $^{18}$F-FDG uptake is not specific and accumulates strongly at sites with increased glucose metabolism such as inflammatory lesions, brain, kidneys, and urinary tract. Furthermore, $^{18}$F-FDG cannot distinguish infections from other conditions such as cancer and inflammation, making it nonspecific for bacterial imaging (*6–8*). Therefore, there is a need for rapid whole-body imaging techniques that can localize a pathogen with specificity and provide a quantitative readout of disease-burden response to treatment.

Besides the lack of specific probes for bacterial infection, another major limitation preventing the effective treatment of bacterial infections is the inability to image them in vivo with the appropriate accuracy and sensitivity. Currently, most imaging agents can detect a high burden of bacteria only in vivo ($>10^9$) (*9*). Consequently, bacterial infections can be diagnosed only after they have become systemic or have caused significant anatomic tissue damage, a stage at which they are challenging to treat because of the high bacterial burden ($>8.3$ log10 colony-forming units [CFUs]/mL) (*10*). Therefore, there is a great need to develop imaging agents with high selectivity and sensitivity.

Sorbitol, known as a "sugar-free" sweetener, is a metabolic substrate for Enterobacteriaceae. 2-$^{18}$F-fluorodeoxysorbitol ($^{18}$F-FDS), a positron-emitting analog of sorbitol, was first prepared by Li et al. for tumor imaging but was found not to accumulate in cancer cells in vitro (300-fold lower accumulation than that of $^{18}$F-FDG) (11). A recent study indicated that $^{18}$F-FDS specifically accumulates in several strains of gram-negative bacteria but not gram-positive bacteria, with 1,000-fold higher uptake in *Escherichia coli* than in mammalian cells. PET/CT imaging results showed that $^{18}$F-FDS accumulated in the thigh of a mouse infected with live *E. coli* but not in one treated with dead *E. coli*, whereas there was no significant difference in $^{18}$F-FDG uptake between the two thighs, indicating the high selectivity of $^{18}$F-FDS (12). Thus $^{18}$F-FDS is a promising PET radiotracer for imaging bacterial infection.

In our current study, we used $^{18}$F-FDS to image mouse lung infection caused by *K. pneumoniae*. Our objectives were 3-fold: first, to demonstrate that $^{18}$F-FDS can be used as an imaging biomarker to monitor disease progression caused by *K. pneumoniae* bacterial infection in a mouse lung infection model; second, to demonstrate that $^{18}$F-FDS, in comparison with $^{18}$F-FDG, is a pathogen-specific marker with high specificity in distinguishing bacterial infection caused by *K. pneumoniae* from sterile lung inflammation; and third, to validate that $^{18}$F-FDS is a potential radiopharmaceutical for imaging bacterial infection by correlating its uptake to bacterial growth measured by bioluminescent imaging (BLI).

## MATERIALS AND METHODS

Unless noted otherwise, all chemicals were of analytic grade and purchased from Sigma-Aldrich. $^{18}$F-FDG was purchased from PETNET Solutions Inc. The *K. pneumoniae* strain (ATCC 43816) was kindly provided by Virginia Miller, of the University of North Carolina at Chapel Hill.

$^{18}$F-FDS was prepared from commercially available $^{18}$F-FDG using a published method (12). Briefly, $^{18}$F-FDG was mixed with 5 mg of solid sodium borohydride at 35°C for 15 min and then quenched with acetic acid, after which the pH was adjusted to 7.4 with sodium bicarbonate. The product was collected by passage through a Sep-Pak Alumina N cartridge (Waters) and 0.2-mm filter. Radiochemical purity was verified by thin-layer chromatography.

### Bacterial Uptake Assays

The bioluminescent *K. pneumoniae* strains (JSKP001 strains), which were created by the insertion of a lux operon between *fusA* and *yeeF* genes using 2-stage allelic exchange mutagenesis as described previously (1), were cultured routinely in LB broth (Lennox) agar plates at 37°C. *K. pneumoniae* was subcultured overnight for 3 h at 37°C. CFUs were enumerated by dilution and plated onto solidified LB broth (Lennox) medium (1). Radiotracer uptake assays were performed by incubating different numbers of bacterial cultures ($10^4$–$10^9$ bacterial CFUs in 10-fold increments, $n = 6$ each) with either $^{18}$F-FDS (20 kBq/mL) or $^{18}$F-FDG at 37°C for 2 h. As a control, heat-killed (90°C for 30 min) bacteria were similarly incubated with each radiotracer. Bacteria were pelleted by centrifugation and washed twice with phosphate buffer, and radioactivity was counted using an automated γ-counter. Percentage uptake in bacteria was calculated by 100 × (counts in pellet/total counts).

### Animal Models

Murine infection studies were approved by the University of Louisville Institutional Animal Care and Use Committee in accordance with the National Institutes of Health guidelines. Female C57

BL mice (8–10 wk old; Charles River) were inoculated with live *K. pneumoniae* ($10^5$ CFUs/mL) or dead *K. pneumoniae* ($10^8$ CFUs/mL) using a previously published intubation-mediated intratracheal instillation method (13).

### BLI

For mice infected with live bacteria, BLI was performed using Photon Imager (BioSpace) at 4 different time points: baseline control before inoculation and days 1, 2, and 3 after inoculation. In preparation for in vivo imaging, the mice were anesthetized with 2%–3% isoflurane in an oxygen-filled induction chamber. Once anesthetized, the mice were placed in an imaging chamber connected to an anesthesia delivery system and kept at 1%–2% isoflurane. Images were acquired according to the manufacturer's instructions. The ex vivo BLI images of the major organs were acquired immediately after euthanasia before γ-counting. In vivo BLI signals were quantified from a selected region of interest (ROI) and expressed as ph/s. The in vivo lung BLI ROI was used to evaluate the degree of infection.

### PET/CT Imaging in Mice with Infection

Twelve mice were imaged by PET/CT on days 1, 2, and 3 after inoculation to monitor disease progression ($n = 12$ for each tracer: $^{18}$F-FDS or $^{18}$F-FDG). A 7.4-MBq dose of a radiotracer ($^{18}$F-FDS or $^{18}$F-FDG) was injected intravenously into each mouse via the tail vein. The mice were then anesthetized with 1.5% isoflurane and placed at the center of the field of view. PET imaging was performed 1 h after inoculation using a microPET-R4 scanner (Siemens) and then followed by CT (microCAT-II; Siemens). Images were reconstructed using an ordered-subsets expectation-maximum algorithm. ROIs were expressed as percentage injected dose (%ID)/g. CT imaging was performed for 10 min immediately after PET imaging for anatomic coregistration and attenuation correction. Nine of the 12 mice were sacrificed immediately after imaging, and then tissues and organs of interest were removed, weighed, and counted. After ex vivo BLI and radioactivity counting, lung tissues were collected for CFU counting. Briefly, the tissues were weighed and homogenized in 1 mL of phosphate-buffered saline, and the cells are lysed with 1% Triton X-100 (The Dow Chemical Company). The diluted samples were quantified after overnight incubation at room temperature. The total CFUs per tissue were estimated using the tissue weight and density.

For another group of 12 mice, PET/CT imaging was performed only when the mice had a fully developed lung infection, as determined by a lung BLI ROI of more than $10^8$. The mice were then immediately sacrificed after imaging ($n = 9$). All other procedures were the same as described above.

### PET/CT Imaging in Mice with Inflammation

For mice with lung inflammation ($n = 5$ for each tracer: $^{18}$F-FDS or $^{18}$F-FDG), PET/CT imaging was performed using a procedure similar to that for the infected group, except that one more time point—day 4 after inoculation—was added.

### Statistical Analyses

Statistical comparisons were performed using a 2-tailed Mann–Whitney U or Kruskal–Wallis (for multiple comparisons) test (GraphPad Software Inc.). A $P$ value of less than 0.05 was considered statistically significant.

## RESULTS

### Bacterial Uptake Assays

Uptake of $^{18}$F-FDS and $^{18}$F-FDG was proportional to the number of bacteria in vitro, reaching a plateau at about $10^8$ CFUs/mL. Both radiotracers could detect as few as $10^6$ CFUs/mL in vitro. Neither $^{18}$F-FDS nor $^{18}$F-FDG accumulated in dead bacteria (Fig. 1).
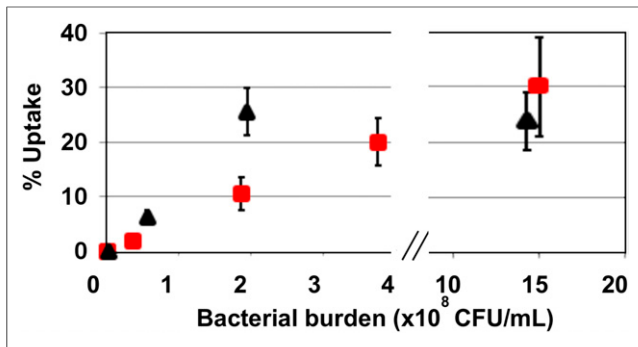
**FIGURE 1.** In vitro uptake of $^{18}$F-FDS (▲) and $^{18}$F-FDG (■) in different CFUs of bacteria ($n = 6$). Either $^{18}$F-FDS or $^{18}$F-FDG (20 kBq/mL) was incubated with different numbers of bacterial culture at 37°C for 2 h. $^{18}$F-FDS uptake plateaued more quickly than $^{18}$F-FDG and remained there for a larger range of bacterial burden.

In vitro BLI showed that light intensity was proportional to the number of live bacteria, but no light was detected for dead bacteria.

### BLI and PET/CT Imaging in Mice with Infection

For mice that could survive 3 d after inoculation, disease progression was monitored over the time course. Both BLI and PET imaging revealed the increase in lung infection over time (Fig. 2). BLI detected noticeable lung infection on day 2 after inoculation and significantly greater infection on day 3. Baseline imaging before inoculation showed no focal areas of lung consolidation on CT and low uptake in the lung for both $^{18}$F-FDS and $^{18}$F-FDG. On day 2, an area of lung consolidation was identified on CT, with a corresponding 2.5-fold increase over baseline for both PET radiotracers. On day 3, widespread areas of patchy lung consolidation were observed on CT, with a drastic increase in uptake for $^{18}$F-FDS and $^{18}$F-FDG (9.2- and 3.9-fold, respectively). These results indicated that the uptake of both radiotracers is proportional to bacterial growth.

On the basis of quantification of lung tissue, correlations among BLI, CFUs, and PET were calculated. The correlation equation between lung BLI and CFUs was $y = 0.91x^{-0.20}$ ($r = 0.95$) ($y$: bioluminescence intensity in unit of log ph/s; $x$: log CFUs). Correlations between ROIs and PET ROIs for $^{18}$F-FDS and $^{18}$F-FDG are shown in Figure 3. The equations were $y = 0.81x^{-4.7}$ ($r = 0.85$) and $y = 2.5x^{-7.3}$ ($r = 0.63$) for $^{18}$F-FDS and $^{18}$F-FDG, respectively ($y$: tracer uptake in lung with unit of % ID/g; $x$: bioluminescence intensity in lung with unit of log ph/s). $^{18}$F-FDS correlated better with BLI than did $^{18}$F-FDG, indicating a better correlation with CFUs. On the basis of day 2 PET imaging, the minimum CFUs that $^{18}$F-FDS and $^{18}$F-FDG could detect in vivo was $10^{7.1}$ and $10^{7.8}$, respectively.

The results of the biodistribution studies for $^{18}$F-FDS and $^{18}$F-FDG are shown in Figure 4. Radioactivity localized mainly in kidney and lung for $^{18}$F-FDS but in brain, heart, spleen, and lung for $^{18}$F-FDG. Uptake in lung was $4.44 \pm 1.95$ and $9.95 \pm 1.93$ %ID/g for $^{18}$F-FDS and $^{18}$F-FDG, respectively. The infected lung-to-heart ratio was 1.6 and 0.7 for $^{18}$F-FDS and $^{18}$F-FDG, respectively—values that were similar to those obtained by PET ROI analysis.
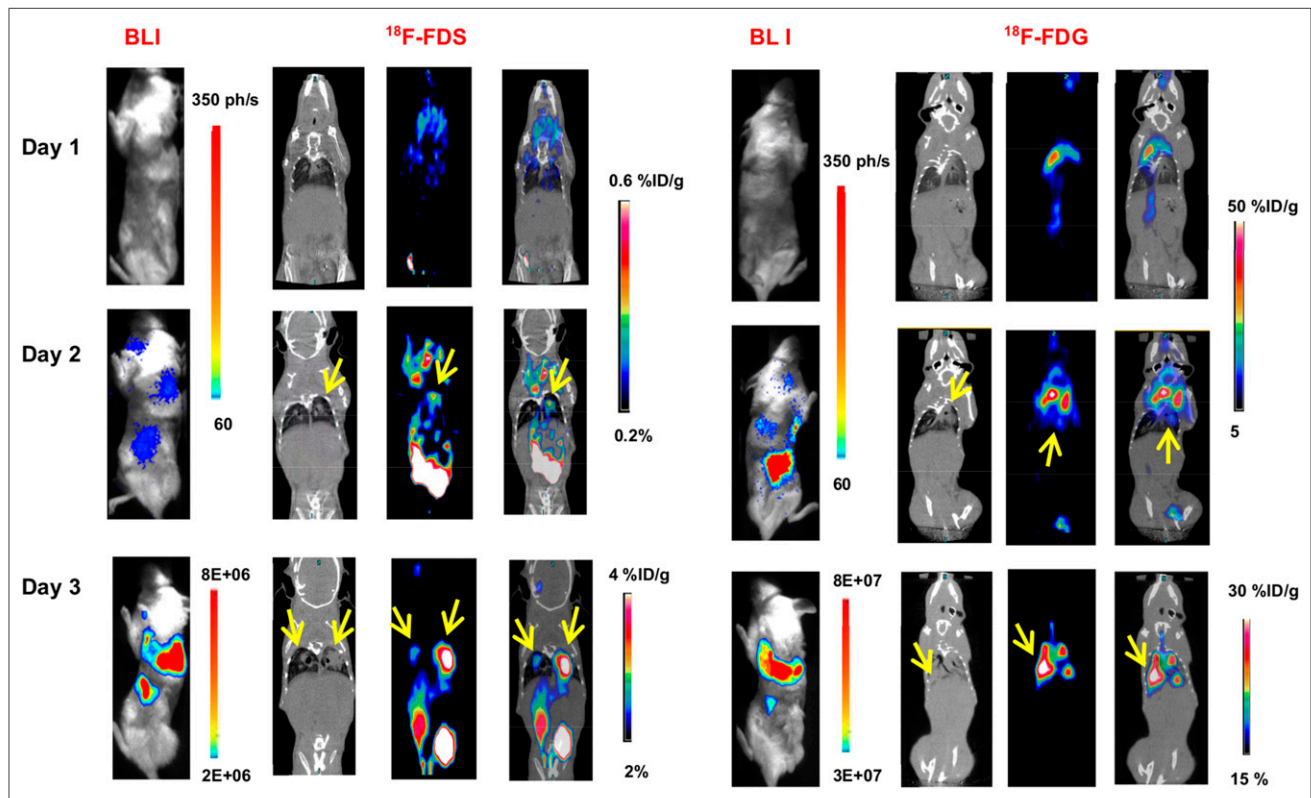


**FIGURE 2.** Representative BLI and PET/CT images of $^{18}$F-FDS and $^{18}$F-FDG in mouse lung infected with *K. pneumoniae* on days 1, 2, and 3 after inoculation. Arrows indicate area of consolidation caused by bacterial infection. BLI showed mild lung infection on day 2 and significantly greater infection on day 3. PET/CT showed increased uptake over the infection time for both $^{18}$F-FDS and $^{18}$F-FDG. On day 3, a drastic increase in $^{18}$F-FDS and $^{18}$F-FDG uptake was seen, with widespread areas of patchy lung consolidation on CT.
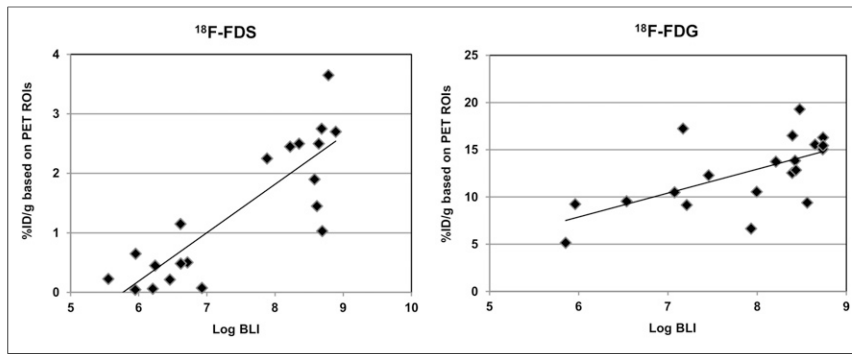
**FIGURE 3.** Correlation between PET and BLI ROIs in infected lung using $^{18}$F-FDS and $^{18}$F-FDG. Correlation was found to be $y = 0.81x^{-4.7}$ ($r = 0.85$) and $y = 2.5x^{-7.3}$ ($r = 0.63$) for $^{18}$F-FDS and $^{18}$F-FDG, respectively ($y$-axis: tracer uptake in lung; $x$-axis: bioluminescence light intensity in lung). Correlation with BLI was better with $^{18}$F-FDS than with $^{18}$F-FDG, indicating a better imaging biomarker to track CFUs.

Ex vivo BLI for major organs (Fig. 4) found the highest bacterial accumulation to be in lung, with 50-fold lower uptake in liver.

### PET/CT Imaging with $^{18}$F-FDS and $^{18}$F-FDG in Mice with Inflammation

For imaging with $^{18}$F-FDG, CT images showed clear inflammation on days 2 and 3, with correspondingly high $^{18}$F-FDG uptake on PET. On day 4, the degree of inflammation was reduced, as inferred by a decrease in $^{18}$F-FDG uptake (Fig. 5A). For imaging with $^{18}$F-FDS, CT images also showed noticeable inflammation, especially on day 3, but no significant uptake on PET was detected on any day (Fig. 5B). PET



**FIGURE 4.** Biodistribution of $^{18}$F-FDG and $^{18}$F-FDS in infected mice ($n = 9$) and representative ex vivo BLI image. Mice were sacrificed after imaging at 2 h after inoculation. Radioactivity was localized mainly in kidney and lung for $^{18}$F-FDS but mainly in brain, heart, spleen, and lung for $^{18}$F-FDG. Ex vivo BLI for major organs demonstrated highest bacterial accumulation in lung, with 50-fold lower accumulation in liver.

quantification showed that the uptake ratio for infected lung–to–inflamed lung on day 3 was 1.7 and 8.5 for $^{18}$F-FDG and $^{18}$F-FDS, respectively.

### DISCUSSION

Enterobacteriaceae rank seventh among the 10 most common pathogens and third among the most common gram-negative pathogens causing device-associated and procedure-associated health care–associated infections (2). The rising resistance of *K. pneumoniae* infections to multiple antibiotics, making the treatment challenging, has emerged as a major concern in hospitals, nursing homes, and other health care settings (13). Therefore, early diagnosis of these infections is critical. In addition, tracking resistant bacteria such as *K. pneumoniae* is 1 of 4 core actions that will help fight these deadly infections and promote the development of new antibiotics and new diagnostic tests for resistant bacteria (14).

However, it is challenging to diagnose *K. pneumoniae* infections at an early stage, because the symptoms look identical to those of a variety of other illnesses, such as cancer and inflammation (15). Furthermore, discrimination of generalized inflammation from infection is not easy, primarily because of similarities in immune response generated by tissue damage or chronic insult. The currently used imaging techniques are not specific to bacteria but rely largely on the detection of inflammation associated with infection (16). Thus, it is extremely important to develop an imaging approach capable of discriminating bacterial infection from inflammation and other diseases.

Noninvasive imaging can provide realtime in vivo monitoring of the progression of infection that may give insight into the mechanisms that modulate disease progression. PET is a highly sensitive (pmol/L) technique that can be used to detect the presence of specific target molecules in sites of interest. There is still a shortage of effective bacterial infection–specific imaging approaches such as antibodies, antimicrobial peptides, and antibiotics and small molecules (e.g., zinc(II)-dipicolylamine derivatives and the thymidine kinase substrate 1-(2-deoxy-2-fluoro-β-D-arabinofuranosyl)-5-iodoracil) (17–20)). $^{18}$F-FDS has been shown not only to differentiate bacterial infection from sterile inflammation but also to discriminate gram-negative bacteria from gram-positive pathogens, cancer cells, and mammalian cells (12). Moreover, a recent study on healthy volunteers using $^{18}$F-FDS did not detect adverse effects, holding potential for clinical application (21). In our study, we used $^{18}$F-FDS to image lung infection in mice induced with *K. pneumoniae*, which was engineered to emit bioluminescent light without the use of exogenous luciferin. For the first
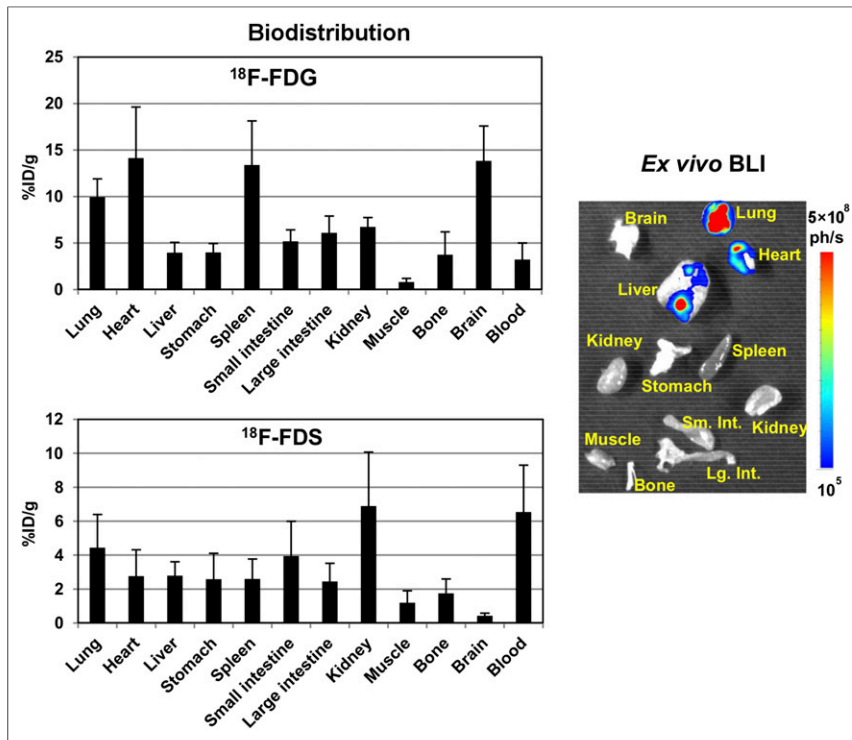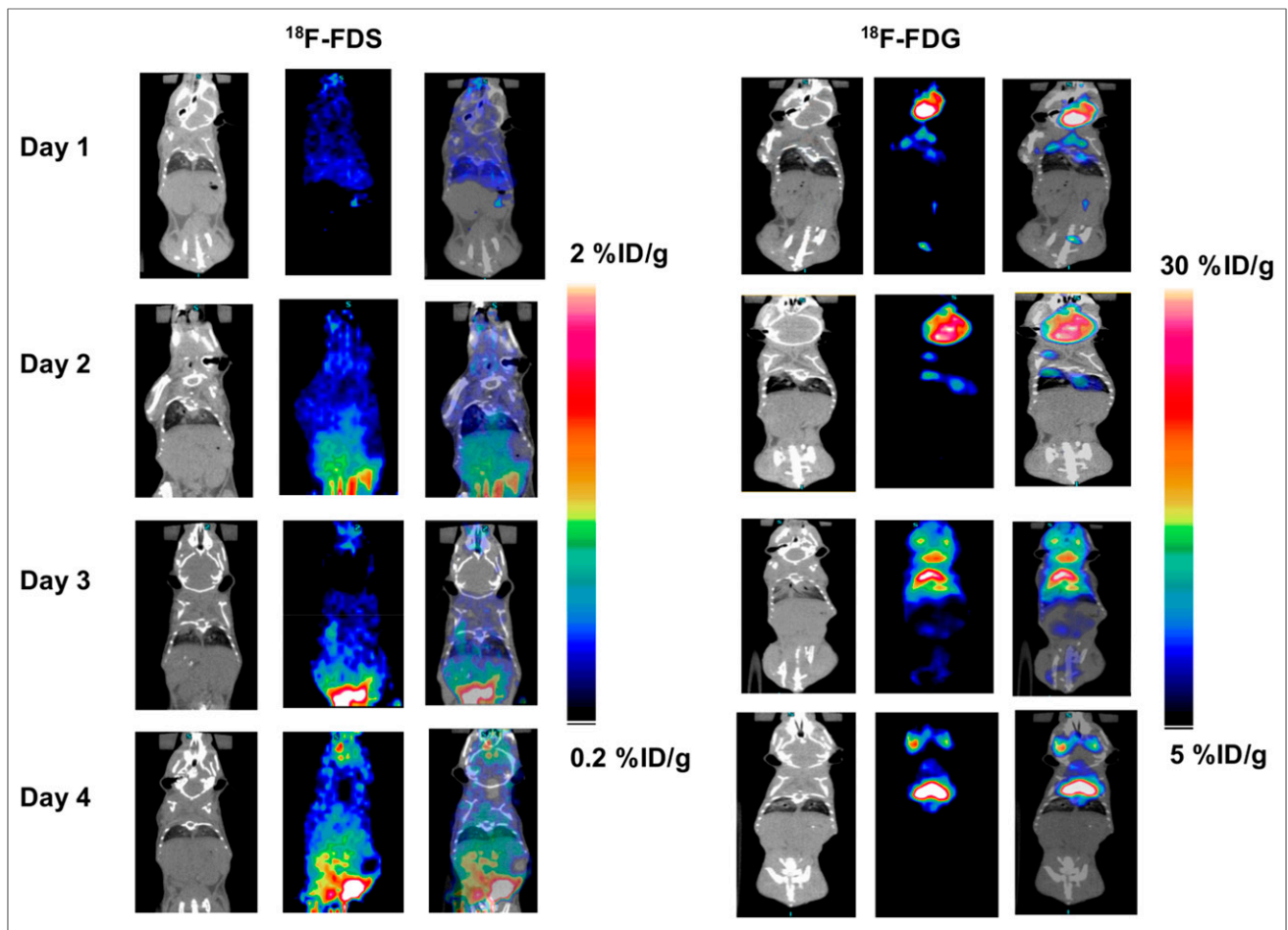
**FIGURE 5.** Representative PET/CT images of $^{18}$F-FDS and $^{18}$F-FDG in inflamed mice. Mice were inoculated with dead *K. pneumoniae* ($10^8$ CFUs/mL). Imaging was performed on days 1, 2, 3, and 4 using $^{18}$F-FDG and $^{18}$F-FDS. CT images showed clear inflammation on days 2 and 3, with correspondingly high $^{18}$F-FDG uptake on PET. No significant uptake of $^{18}$F-FDS was detected on any of those 4 days.

time, to our knowledge, we showed the feasibility of using in vivo BLI and $^{18}$F-FDS PET/CT to track the progression of *K. pneumoniae* infection over time. We also demonstrated that $^{18}$F-FDS was more specific than $^{18}$F-FDG in differentiating *K. pneumoniae* infection from sterile lung inflammation. To determine the detection threshold for $^{18}$F-FDG and $^{18}$F-FDS in vitro, we performed in vitro tracer uptake experiments using different bacterial loads (live bacteria vs. heat-killed dead bacteria). As shown in Figure 1, $^{18}$F-FDS could detect as few as $10^6$ bacteria in vitro, and $^{18}$F-FDG showed a similar detection sensitivity.

We performed in vivo BLI and PET/CT imaging on mice to assess the potential of $^{18}$F-FDS to be an imaging biomarker to monitor the progression of lung infection. Over the time course of infection, in vivo BLI showed that light intensity increased in the lungs, indicating the development of lung infection due to bacterial dissemination over time. At day 1 after inoculation, there was no bioluminescence signal in the lung, despite the presence of approximately $10^6$ bacteria. This should be related to a threshold detection limit of BLI in vivo. By day 2, the bioluminescence signal and tracer accumulation in the lung were clearly visible, and they increased significantly by day 3 (Fig. 2), indicating that $^{18}$F-FDS might be a suitable radiopharmaceutical for monitoring the progression of bacterial infection. The preliminary data using BLI screening suggested a survival rate of 50% throughout 3 d after inoculation. Our original goal was to have at least 5 mice on day 3 after inoculation; for each radiotracer, we

started with 12 mice on day 1 after inoculation, lost about 10%–20% of the mice on day 2, and were left with only 3 mice on day 3. We later noticed that the cumulative stress as the result of frequent tail vein injections, anesthesia during PET/CT scans, and bacterial infection was likely the contributing factor to the overall survival rate of the infected mice. Furthermore, the response of the mice to lung infection varied. A severe infection developed by day 2 in some mice but not until day 3 in most mice. Thus, we used BLI as a screening tool to select mice with adequate lung infection (lung BLI ROIs $> 10^8$ ph/s) for PET/CT imaging. Immediately after imaging, the mice were sacrificed for biodistribution measurement. This strategy greatly increased the number of mice with lung infection for PET/CT imaging.

Light intensity measured by BLI showed an excellent correlation with CFUs, or bacterial growth ($r = 0.95$). Although $^{18}$F-FDS and $^{18}$F-FDG uptake correlated well with BLI and CFUs, $^{18}$F-FDS/PET correlated better with BLI than did $^{18}$F-FDG/PET ($r = 0.85$ vs. 0.63), indicating that $^{18}$F-FDS might be better than $^{18}$F-FDG as an imaging biomarker to track bacterial growth.

After imaging, the mice were sacrificed for ex vivo BLI and biodistribution studies to confirm the relationship between uptake and bacterial infection in different organs. Ex vivo BLI detected bacterial accumulation predominantly in lung ($>10^8$ ph/s) and slightly in heart and liver ($\sim 10^6$) (Fig. 4). Subsequently, the biodistribution for both radiotracers also showed high lung uptake. For $^{18}$F-FDG, high uptake

was also seen in brain, heart, and spleen, indicating the nonspecificity of this radiotracer. $^{18}$F-FDG commonly showed high uptake in brain and heart in mice (22), and high spleen uptake was probably due to an inflammatory host response to bacteria (23). The uptake pattern of $^{18}$F-FDS was more specific than that of $^{18}$F-FDG. Lung had the highest uptake, in addition to kidney and blood. High kidney uptake was mostly due to the clearance pathway of $^{18}$F-FDS but not bacterial uptake. A long residence time of $^{18}$F-FDS in the blood implies that $^{18}$F-FDS might require a waiting period, but the advantage of late imaging will decrease if uptake in the lung is diminished. Additionally, we found that uptake in major organs varied greatly among mice with different levels of infection. For healthy mice or mice with mild infection (lung BLI ROIs: $10^4$–$10^6$ ph/s), more than 90% of $^{18}$F-FDS was cleared from all major organs at 2 h after inoculation, with the blood level reaching as low as 0.08 %ID/g. Although further investigation is warranted, a high lung-to-baseline ratio of 9.3 based on PET imaging (Fig. 2) and a high lung-to-muscle ratio of 3.7 based on biodistribution studies (Fig. 4) suggest that $^{18}$F-FDS imaging at 1 h after radiotracer administration might be sufficient for imaging bacterial infection. Moreover, the biodistribution data from Figure 4 demonstrate much lower uptake of $^{18}$F-FDS in heart, with a lung-to-heart ratio of 1.6 instead of 0.7, compared with $^{18}$F-FDG.

To determine whether $^{18}$F-FDS is more specific than $^{18}$F-FDG in differentiating lung infection from lung inflammation, we performed in vivo BLI and PET/CT imaging using these two radiotracers in mice infected with *K. pneumoniae* in the lung and mice with sterile lung inflammation caused by dead *K. pneumoniae*. PET quantification (Fig. 5) showed no significant uptake difference between these two groups for $^{18}$F-FDG ($P > 0.05$) but a significant difference for $^{18}$F-FDS ($P < 0.001$), as is consistent with the biodistribution data. Histopathologic evaluation of the lungs inoculated with dead bacteria confirmed the presence of the inflammatory cells in both groups of mice. This finding confirms that $^{18}$F-FDS can be used to specifically differentiate bacterial infection from sterile inflammation, an ability that is extremely critical for early and effective treatment in the clinic. Our findings are consistent with those of a published study (12) that also used $^{18}$F-FDS to image lung infection caused by *K. pneumoniae,* but the strain of bacteria used in that study was the ATCC 700721 strain, better known as MGH 78578, which is relatively avirulent and has a 50% lethal dose of $10^8$ CFUs (23). In contrast, we used a highly virulent strain (50% lethal dose, 100 CFUs) called ATCC 43816 (13). This difference explains why the animals in the other study were inoculated with a higher dose of bacteria but developed only mild lung infection on day 5 after inoculation whereas our animals started to develop lung infection on day 2, with a mortality rate of about 10%–20%, and infection was fully developed on day 3, with a survival rate of 30%–40%. This finding further highlights the importance of early and effective diagnosis of this type of infection with such a high mortality rate. It is worth noting that the *K. pneumoniae* bacteria used in our study were engineered to emit light, and it was thus possible to use bioluminescence imaging to follow bacterial growth in vivo.

## CONCLUSION

The degree of lung infection measured by BLI correlated better with $^{18}$F-FDS uptake than with $^{18}$F-FDG uptake. Both $^{18}$F-FDS and $^{18}$F-FDG showed a reasonable detection threshold for imaging bacterial infection. $^{18}$F-FDS was more specific than $^{18}$F-FDG in differentiating *K. pneumoniae* lung infection from lung inflammation. Therefore, $^{18}$F-FDS can be considered a promising imaging biomarker for early diagnosis of *K. pneumoniae* lung infections in mice. Currently, the imaging modalities used to investigate patients carrying or suspected of having lung infection are chest radiography and CT, but CT is much

more sensitive and specific than chest radiography. However, the interpretation of CT images for lung disorders can be complex if the differential diagnosis needs to distinguish between inflammation and infection. Thus, $^{18}$F-FDS PET/CT can be used initially for follow-up after an inconclusive CT diagnosis for suspected lung infection. As proven clinical data accumulate over time, $^{18}$F-FDS PET/CT can potentially become a new clinical standard for confirming lung infection.

## DISCLOSURE

No potential conflict of interest relevant to this article was reported.

## REFERENCES

1. Fodah RA, Scott JB, Tam HH, et al. Correlation of *Klebsiella pneumonia* comparative genetic analysis with virulence profiles in a murine respiratory disease model. *PLoS One.* 2014;9:e107394.
2. Hidron AI, Edwards JR, Patel J, et al. NHSN annual update: antimicrobial-resistant pathogens associated with health care-associated infections: annual summary of data reported to the National Healthcare Safety Network at the Centers for Disease Control and Prevention, 2006-2007. *Infect Control Hosp Epidemiol.* 2008;29:996–1011.
3. Pourakbari B, Mamishi S, Zafari J. Evaluation of procalcitonin and neopterin level in serum of patients with acute bacterial infection. *Braz J Infect Dis.* 2010;14:252–255.
4. Sanchez GV, Master RN, Clark RB, et al. *Klebsiella pneumoniae* antimicrobial drug resistance, United States, 1998-2010. *Emerg Infect Dis.* 2013;19:133–136.
5. Hansell DM, Bankier AA, MacMahon H, et al. Fleischner Society: glossary of terms for thoracic imaging. *Radiology.* 2008;246:697–722.
6. Jonsson CB, Camp JV, Wu A, et al. Molecular imaging reveals a progressive pulmonary inflammation in lower airways in ferrets infected with 2009 H1N1 pandemic influenza virus. *PLoS One.* 2012;7:e40094.
7. Davis SL, Nuermberger EL, Um PK, et al. Noninvasive pulmonary [$^{18}$F]-2-fluoro-deoxy-D-glucose positron emission tomography correlates with bactericidal activity of tuberculosis drug treatment. *Antimicrob Agents Chemother.* 2009;53:4879–4884.
8. Kumar R, Nadig MR, Balakrishnan V, Bal C, Malhotra A. FDG-PET imaging in infection and inflammation. *Indian J Nucl Med.* 2006;21:104–113.
9. Leevy WM, Gammon ST, Johnson JR, et al. Noninvasive optical imaging of *Staphylococcus aureus* bacterial infection in living mice using a Bis-DPA-Zinc(II) affinity group conjugated to a NIR fluorophore. *Bioconjug Chem.* 2008;19:686–692.
10. König C, Simmen HP, Blaser J, et al. Bacterial concentrations in pus and infected peritoneal fluid: implications for bactericidal activity of antibiotics. *J Antimicrob Chemother.* 1998;42:227–232.
11. Li ZB, Wu Z, Cao Q, et al. The synthesis of $^{18}$F-FDS and its potential application in molecular imaging. *Mol Imaging Biol.* 2008;10:92–98.
12. Weinstein EA, Ordonez AA, DeMarco VP, et al. Imaging Enterobacteriaceae infection in vivo with $^{18}$F-fluorodeoxysorbitol positron emission tomography. *Sci Transl Med.* 2014;6:259ra146.
13. Lawrenz MB, Fodah RA, Gutierrez MG, Warawa J. Intubation-mediated intratracheal (IMIT) instillation: a noninvasive, lung-specific delivery system. *J Vis Exp.* 2014;(93):e52261.
14. *Antibiotic resistance threats in the United States, 2013.* Atlanta, Georgia: Centers for Disease Control and Prevention; 2013:31.
15. Ning X, Seo W, Lee S, et al. PET imaging of bacterial infections with fluorine-18-labeled maltohexaose. *Angew Chem Int Ed Engl.* 2014;53:14096–14101.
16. Eggleston H, Panizzi P. Molecular imaging of bacterial infections in vivo: the discrimination between infection and inflammation. *Informatics.* 2014;1:72–99.
17. Bhargava KK, Gupta RK, Nichols KJ, Palestro CJ. In vitro human leukocyte labeling with $^{64}$Cu: an intraindividual comparison with $^{111}$In-oxine and $^{18}$F-FDG. *Nucl Med Biol.* 2009;36:545–549.
18. Nazari B, Azizmohammadi Z, Rajaei M, et al. Role of $^{99m}$Tc-ubiquicidin 29-41 scintigraphy to monitor antibiotic therapy in patients with orthopedic infection: a preliminary study. *Nucl Med Commun.* 2011;32:745–751.
19. Smith BA, Xiao S, Wolter W, Wheeler J, Suckow MA, Smith BD. In vivo targeting of cell death using a synthetic fluorescent molecular probe. *Apoptosis.* 2011;16:722–731.
20. Bettegowda C, Foss CA, Cheong I, et al. Imaging bacterial infections with radiolabeled 1-(2′-deoxy-2′-fluoro-β-D-arabinofuranosyl)-5-iodouracil. *Proc Natl Acad Sci USA.* 2005;102:1145–1150.
21. Yao S, Xing H, Zhu W, et al. Infection imaging with $^{18}$F-FDS and first-in-human evaluation. *Nucl Med Biol.* 2016;43:206–214.
22. Shreve PD, Anzai Y, Wahl RL. Pitfalls in oncologic diagnosis with $^{18}$F-FDG PET imaging: physiologic and benign variants. *Radiographics.* 1999;19:61–77.
23. Aoshi T, Zinselmeyer BH, Konjufca V, et al. Bacterial entry to splenic white pulp initiates antigen presentation to CD8+ T cells. *Immunity.* 2008;29:476–486.